Hindawi
Advances in Civil Engineering
Volume 2019, Article ID 1827479, 15 pages
https://doi.org/10.1155/2019/1827479

Research Article

Novel Excavation and Construction Method for a Deep Shaft Excavation in Ultrathick Aquifers

Chengyong Cao, Chenghua Shi, Linghui Liu, Jianwen Liu, Mingfeng Lei, Yuexiang Lin, and Yichao Ye

School of Civil Engineering, Central South University, Changsha 410075, China

Correspondence should be addressed to Chenghua Shi; csusch@163.com and Jianwen Liu; jwenliu@csu.edu.cn

Received 2 July 2019; Revised 13 August 2019; Accepted 29 August 2019; Published 30 September 2019

Academic Editor: Hossein Moayedi

Dewatering using the dewatering systems composed of diaphragm walls and pumping wells is commonly adopted for deep excavations that are undertaken in deep aquifers. However, dewatering can sometimes induce environmental problems, especially when diaphragm walls cannot effectively cut off the aquifers. This paper mainly presents an innovative excavation technique combining dewatering excavation and underwater excavation without drainage, which is employed for a deep shaft excavation in ultrathick aquifers (up to 60–70 m thick aquifer) in Fuzhou, China. The shaft excavation with the depth of 41.6 m below the ground surface (BGS) is divided into two major phases, that is, (1) the first part of the excavation (the depth of 23.6 m BGS) is conducted by the way of conventional dewatering and braced excavation (Phase I) and (2) the second excavation with the depth of 23.6 m to 41.6 m BGS is carried out by the novel underwater excavation without drainage technique (Phase II). Field monitoring results show that the ratios of maximum ground surface settlement δ_{vm} to the excavation depth H_e in this case ranged from 0.03% to 0.1%. Most of the ratios of maximum lateral wall deflection δ_{hm} to excavation depth H_e are less than 0.1%. All these results are lesser than that predicted by empirical methods, which also confirmed the applicability of this innovative excavation. Thus, this innovative solution can be applicable to other deep excavations that are undertaken in ultrathick aquifers, especially for the excavation of coarse sediments with high permeability.

1. Introduction

With the development of urban infrastructure, a growing number of deep excavation projects have appeared in China [1–5]. In many cases, deep excavation constructions are inevitably built below the water table in urban environments, especially in the coastal regions of China. As a result, dewatering is usually essential to be carried out prior to the excavation to ensure dry and workable conditions inside the excavation and to prevent the excavation bottom uplift or liquefaction when a deep excavation is undertaken in aquifers [6–8]. In general, there are thick aquifers in coastal regions of China, which are composed of sand, gravel, and silt of Quaternary deposits. In this situation, groundwater control is considerably difficult for deep excavations due to the high permeability of soils and heavily thick aquifers [9–11]. Thus, underground enclosures (low-permeability barriers) are commonly used for deep excavations in the presence of groundwater, such as deep cement mixing (DCM) columns, diaphragm walls, and jet grouting columns [12–15]. These underground enclosures are conducted to retain the surrounding soils as well as to prevent lateral groundwater from flooding into the excavations.

So far, many researchers have focused on the issue related to the environmental effect caused by dewatering and excavation during deep excavations [16–20]. Pujades et al. [20, 21] investigated the hydraulic characterization of underground enclosures when used for deep excavations. Generally, when low-permeability barriers are embedded into the impermeable layers, the aquifers will be completely cut off by these enclosed barriers. Under these conditions, dewatering inside an excavation just lowers the groundwater

level, and it cannot cause groundwater drawdown outside the barrier. However, the deeper the excavation depth of the foundation pit, the deeper the depth of underground enclosures required, which thus renders more challenging and uneconomical. In fact, it is unrealistic to employ those completely enclosing barriers for a deep excavation that are undertaken in ultrathick aquifers, and on the contrary, the partially penetrating curtains are the most widely used for deep excavations. Wang et al. [22, 23] analyzed the impact of the partially penetrating underground enclosures on reducing the drawdown and controlling land subsidence outside during excavation. Wu et al. [24] conducted numerical simulations to investigate the mechanism of the blocking effect of partial penetrating curtains embedded in aquifers during dewatering for deep excavations. As a result, the partial penetrating curtains produce positive effect in reducing the groundwater drawdown and water inflow from outside the excavation. Despite many obvious advantages of partial penetrating curtains, it is not without its problem. In such a case that a deep excavation was undertaken in ultrathick aquifers with high permeability, a combination of partial penetrating curtains and pumping wells may not be able to lower the groundwater level inside the excavation and simultaneously minimize the effect of dewatering on the surrounding buildings outside the excavation. Thus, other groundwater control scenarios should be developed for a deep excavation when undertaken in ultrathick aquifers. Currently, dewatering was usually performed prior to the excavation when deep excavations undertaken below the water table, whereas few deep excavations that were conducted using the underwater excavation technique have appeared in the literature.

The objective of this study is to present an innovative excavation combining dewatering excavation and underwater excavation without drainage, which is employed for deep excavation of a shaft excavation that is undertaken in ultrathick aquifer in Fuzhou, China. The 41.6-meter deep excavation of air shaft is divided into two major phases, that is, the first excavation with depth of 23.6 m below the ground surface (BGS) is conducted by the way of dewatering and excavation, and the second excavation with the depth of 23.6 m to 41.6 m BGS is carried out by underwater excavation without drainage technique. In this paper, first, the site characterization and pumping test are introduced. Then, the novel excavation and construction method for the deep shaft excavation is proposed. The effect of the innovative excavation on the soil deformation outside the excavation was analyzed through numerical simulation. Finally, the excavation performance of the deep shaft excavation that was undertaken in the ultrathick aquifer was investigated through real-monitoring data obtained from the field, in order to confirm the applicability of this innovative technique. This case history can provide meaningful references and insights into other projects involving deep excavations that are undertaken in ultrathick aquifers. The innovative solution can also be an alternative for the excavations that are undertaken in deep aquifers when groundwater control is difficult for deep excavations.

2. Site Characterization

2.1. Project Description. The investigated project is an air shaft of Metro line 2, located on the east side of Wulongjiang Wetland Park in Fuzhou, China. Due to the proximity of critical infrastructures, such as flood protection dike, the 3rd ring expressway, a gas station, and several underground service pipes, the surrounding environment of the air shaft is complex, which therefore brings some difficulties and challenges to the construction of the air shaft. The internal length of the air shaft along the subway tunnel alignment is 16.3 m, and the internal width and depth are 24.2 m and 41.6 m, respectively. The cut and cover method is adopted in the air shaft excavation. 120 cm thick and 55 m deep diaphragm walls are used as enclosure structure of the air shaft excavation. The layout of the air shaft is presented in Figures 1(a) and 1(b).

2.2. Geological and Hydrogeological Conditions. The geology of the study site was characterized by means of borehole drilling. Soils at the site of the air shaft are mainly Quaternary deposits and consist of miscellaneous fill (layer ①$_1$), plain fill (layer ①$_2$), medium-coarse sand (layer ②$_5$), and gravel soils (layer ③$_8$). The highly-weathered granite (layer ⑦$_1$) is located below the gravel soil layer. A small amount of silty clay (layer ③$_5$) occurs at the interface between sand and gravel soils and to some extent, which leads to be a decrease in the permeability of soils inside the excavation. Nevertheless, the silty clay layer may have discontinuities, and as a result, gravel soil is directly connected to the sand layer. The depth of the miscellaneous fill layer is from 1.60 to 4.10 m below the ground surface (BGS). A layer of plain fill underlies the miscellaneous fill layer with the depth of 6.3 m to 7.0 m. There is a medium-coarse sand layer with the thickness of 26.4 m to 34.8 m below the plain fill. The next layer is a thin layer of silty clay with the thickness of 0.5 m to 1.0 m. There is a gravel soil layer with the thickness of 26.7 m to 29.3 m underlying the silty clay. The typical geology profile is displayed in Figure 1(c).

The groundwater at the site consists of unconfined water and bedrock fissure water. Since bedrock is located below the ground surface with more than 70 m depth, fissure water has little influence on the air shaft construction. The piezometric head of unconfined water is 3.4–5.6 m BGS and changes with precipitation. The unconfined aquifer mainly consists of medium-coarse sand (layer ②$_5$) and gravel soil (layer ③$_8$). Both of them belong to highly permeable soil, and hydraulic conductivity of sand and gravel soil is 35–55 m/d. Moreover, due to the site adjacent to Wulongjiang River, the groundwater is closely connected with the Wulongjiang River. That brings much challenge to groundwater control for the air shaft excavation.

2.3. Watertightness Assessment Test (WAT). Considering the safety of construction, it is necessary to demonstrate whether the water level inside the air shaft can be lowered below the excavation bottom under the condition of previously

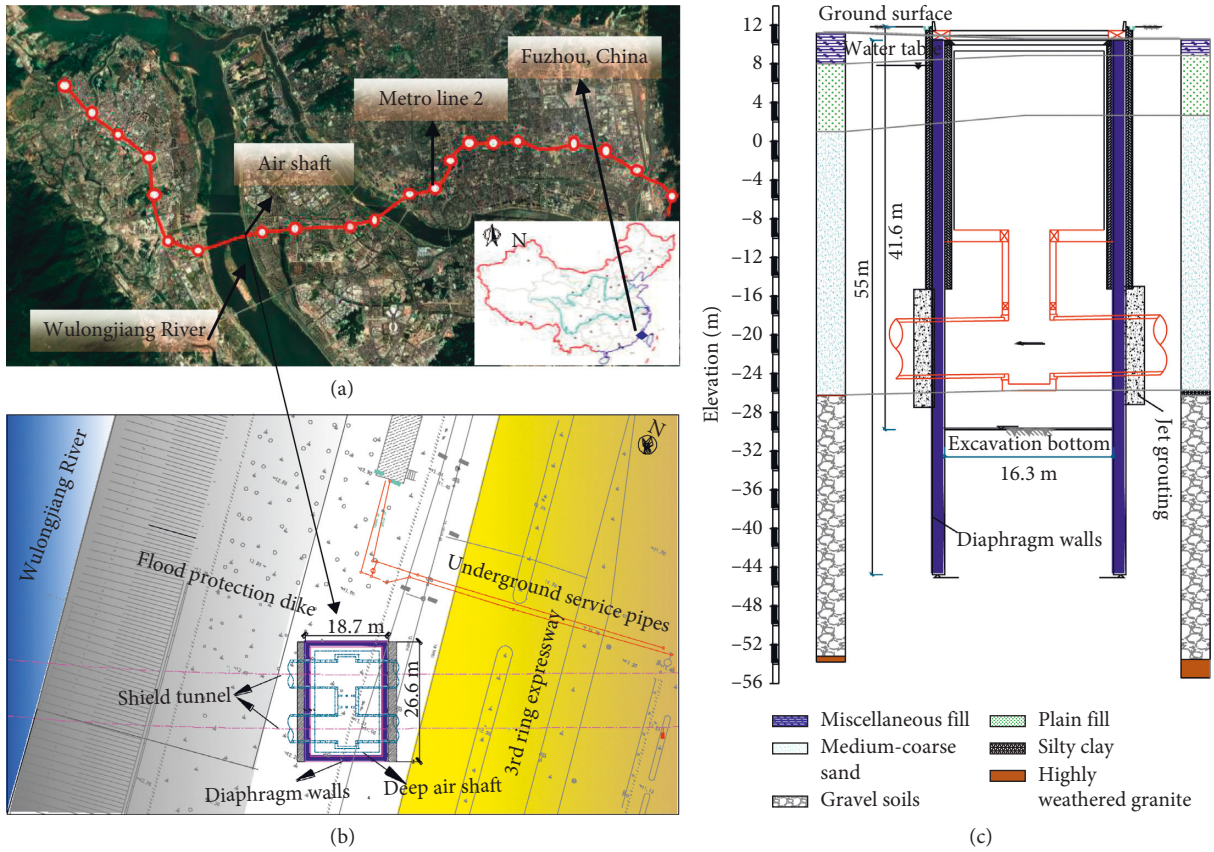

Figure 1: The layout of the air shaft. (a) Geographical location. (b) Plan view. (c) Typical strata profile.

designed dewatering systems (55 m deep diaphragm walls and pumping wells). The watertightness assessment test (WAT) is considered as one of the most convincing means to verify this. Thus, the WAT was carried out prior to the excavation to verify the feasibility of the dewatering system.

Since the air shaft has a small area of 394.46 m^2, a single-well pumping test inside the enclosures is carried out prior to the actual excavation of the air shaft. The layout of pumping tests is shown in Figure 2. The pumping test was started on May 10, 2016, and lasted for 100 hours (50 for pumping and 50 for recovery). Well Y4 was used as a pumping well, and wells Y1 and Y5 as observation wells inside the enclosures. All of the wells were installed to the depth of 38 m below the ground surface. The length of screen of all the wells was 24 m in aquifer. Figures 3(a) and 3(b) display the time-history curves of the pumping rate of pumping well and the variation of drawdown measured in different observation wells during the pumping test, respectively.

As shown in Figures 3(a) and 3(b), the pumping rate of the pumping well was relatively stable and the average value of which was 100 m^3/h during the first 12-hour pumping test. Instead, the drawdown of observation wells changed rapidly. As the drawdown inside the enclosures increased, the pumping rate of the pumping well gradually decreased. After 13-hour pumping test, the water levels of observation wells Y1 and Y5 were 24.37 m and 23.79 m BGS, respectively. Both of them were below the bottom of the Phase I excavation (23.6 m depth BGS), which could meet the requirement of the construction of the Phase I excavation. The pumping rate of the pumping well decreased to be 35 m^3/h and maintained within a narrow range after the 48-hour pumping test. Finally, the water level of two observation wells basically stabled at 29 m depth BGS. The water level outside the excavation did not change significantly during the whole pumping test but changed regularly with the tidal effects. The water level inside the enclosures recovered slowly when the pumping was stopped, which increased by only 9.7 m until 8:00 am on May 21, 2016 (45.5 h after the pumping well stopped).

The results of the single-well pumping test show that the flow rate of the pumping well at the stable period was 35 m^3/h, which was at an acceptable range. Simultaneously, the water level inside the enclosure dropped quickly but recovered slowly. The phreatic water level outside the enclosure did not change during the pumping test (less than 0.5 m). Unfortunately, the water level inside the air shaft can only be lowered at the depth of 29 m BGS under the condition of designed dewatering systems (55 m deep diaphragm walls). This implied there was much challenge in lowering the water level inside to ensure dry and workable conditions for the whole excavation of the air shaft.

3. Methodology

3.1. Proposed Construction Method. Groundwater level inside the enclosures needs to be lowered below the excavation

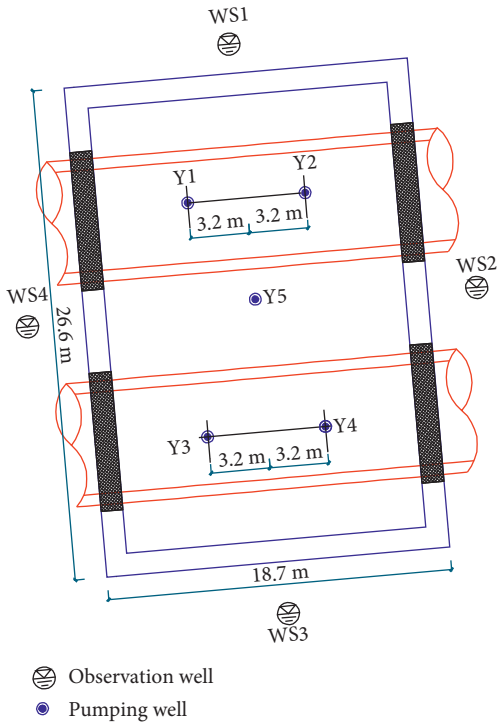

Figure 2: The layout of the pumping test and monitoring points.

bottom to provide dry and workable conditions for the excavation. Nevertheless, the watertightness assessment test has proved that the success of lowering the water level inside below the excavation bottom (at the depth of 41.6 m BGS) cannot be achieved. Since the hydraulic conductivity of gravels at the lower part of the excavation zone is rather large and groundwater recharge comes from the Wulongjiang River rapidly, it is quite difficult to successfully lower the groundwater level below the excavation bottom (at the depth of 41.6 m BGS). Considering such various factors as the geology with high permeability, high head water, the deep excavation close to the Wulongjiang River, critical infrastructures, and underground pipelines surrounding the air shaft, there is a great deal of risk and challenge for the dewatering and excavation.

Furthermore, even though groundwater level inside the excavation was able to be lowered below the excavation bottom, it may cause potential hazard (e.g., quicksand and seepage failure) towards the enclosure structures due to excessive head difference between inside and outside the enclosure. Defects in these enclosure structures are frequent, which can even result in soil being dragged towards the deep excavation and sink holes at the ground surface [19–21].

In view of the abovementioned risk for the air shaft excavation, an innovative scenario for the air shaft excavation of 41.6 m depth was proposed, that is, the whole excavation is divided into two major phases: (1) the excavation of 23.6 m depth is conducted by the way of dewatering excavation (Phase I), and (2) and the second excavation with the depth of 23.6 m to 41.6 m BGS is carried out by underwater excavation without drainage (Phase II).

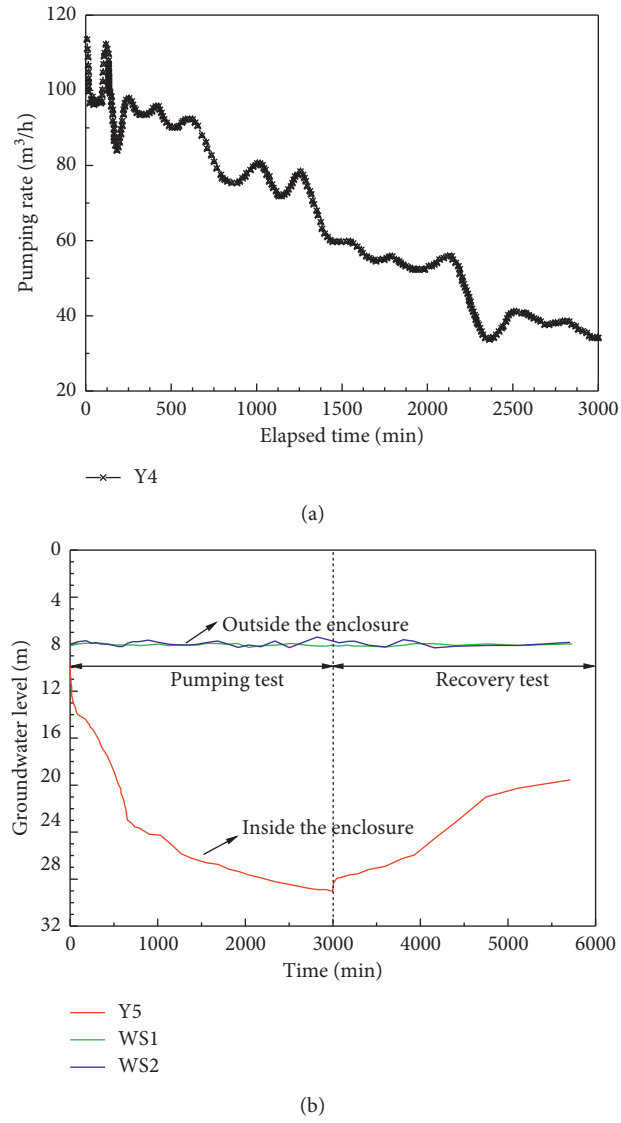

Figure 3: Time-history curves of the pumping test. (a) Pumping rate. (b) Variation of drawdown.

The construction procedure of the air shaft, as presented in Figure 4, included the following: (a) dewatering and Braced excavations up to the depth of 23.6 m BGS; (b) water recharged into the excavation and underwater excavation without drainage by sand-suction machines up to the depth of 41.6 m BGS; (c) underwater bottom-sealing construction; (d) filling in the excavation with low-grade concrete; (e) shields passing through the air shaft; and (f) tunnel segments removal and construction of air channels.

3.2. Numerical Analysis and Assessment. The coupled hydromechanical numerical model was conducted using the finite difference program to investigate the feasibility of this innovative scenario combining dewatering excavation and underwater excavation without drainage. Simultaneously, the effect of the deep excavation on the soil deformation outside the excavation was predicted in advance.

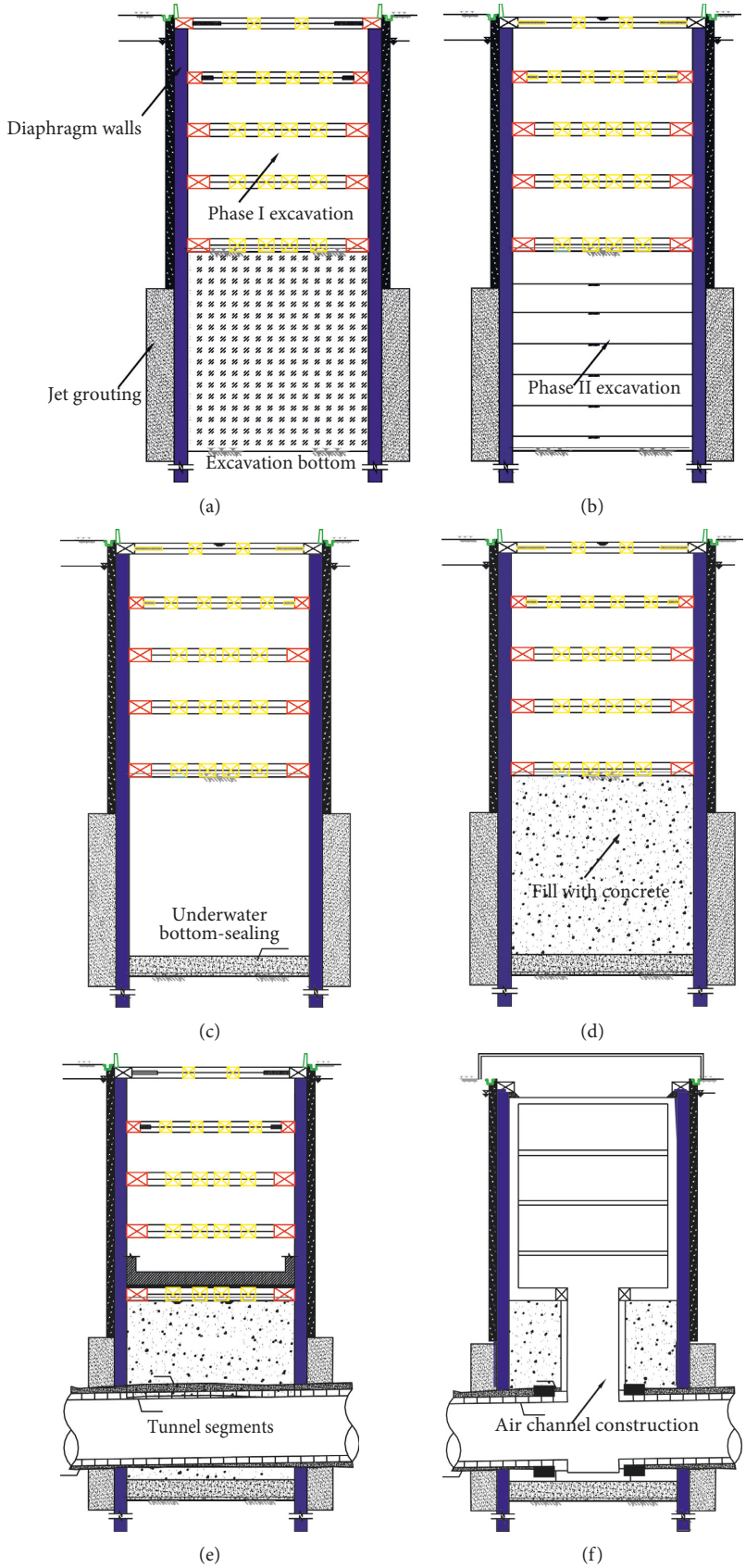

Figure 4: Construction procedure for the air shaft. (a) Dewatering and braced excavations. (b) Underwater excavation without drainage. (c) Underwater bottom-sealing construction. (d) Filling with low-grade concrete. (e) Shields passing through the air shaft. (f) Tunnel segments removed and construction of air channels.

3.2.1. Governing Differential Equations. The governing differential equations characterizing the hydromechanical response of porous materials in FLAC^{3D} are presented as follows [25].

(1) Transport Law. The fluid transport law is given by Darcy's law. For a homogeneous, isotropic solid, and constant fluid density, it is presented as

$$q_i = -k_{ik}\widehat{k}(s)\left[p - \rho_f x_j g_j\right]_{,k}, \tag{1}$$

where q_i is the specific discharge vector; k is the tensor of absolute mobility coefficient of the medium; $\widehat{k}(s)$ is the relative mobility coefficient and related to saturation (s), $\widehat{k}(s) = s^2(3 - 2s)$, and which is zero and one for zero and full saturation, respectively; p is the fluid pressure; ρ_f is the fluid density; and g_j is the gravity vector.

(2) Balance Law. For small deformations, the fluid mass balance can be described as

$$-q_{i,i} + q_v = \frac{\partial \zeta}{\partial t}, \tag{2}$$

where q_v is the volumetric fluid source intensity, ζ is the variation of fluid content of variation of fluid volume per unit volume of porous material due to diffusive fluid mass transport, and t is the time.

The balance of momentum is given in the following form:

$$\sigma_{ij,j} + \rho g_i = \rho \frac{\partial v_i}{\partial t}, \tag{3}$$

where ρ is the bulk density and $\rho = \rho_d + ns\rho_w$ in which ρ_d is the density of the dry matrix, ρ_w is the fluid density, n is the porosity, and s is the saturation.

(3) Constitutive Laws. Changes in the variation of fluid content are closely related to variation in saturation (s), pore pressure (p), and mechanical volumetric strain (ε). The equation describing the response of pore fluid is given as

$$\frac{1}{M}\frac{\partial p}{\partial t} + \frac{n}{s}\frac{\partial s}{\partial t} = \frac{1}{s}\frac{\partial \zeta}{\partial t} - \alpha\frac{\partial \varepsilon}{\partial t}, \tag{4}$$

where M and α are the Biot modulus and Biot coefficient, respectively.

The equation describing the constitutive response of the porous solid is formulated as

$$\widehat{\sigma}_{ij} + \alpha\frac{\partial p}{\partial t}\delta_{ij} = H\left(\sigma_{ij}, \xi_{ij}, \kappa\right), \tag{5}$$

where $\widehat{\sigma}_{ij}$ is the corotational stress rate, H is the functional form of the constitutive law, κ is a history parameter, δ_{ij} is the Kronecker delta, and ξ_{ij} is the strain rate.

In particular, the elastic relations which relate effective stresses to strains are (small strain)

$$\sigma_{ij} - \sigma_{ij}^0 + \alpha\left(p - p^0\right)\delta_{ij} = 2G\varepsilon_{ij} + \left(K - \frac{2}{3}G\right)\varepsilon_{kk}, \tag{6}$$

where the superscript 0 refers to the initial state, ε_{ij} is the strain, and K and G are the bulk and shear moduli of the drained elastic solid, respectively.

(4) Compatibility Equations. The relation between strain rate and velocity gradient is given as

$$\xi_{ij} = \frac{1}{2}\left[v_{i,j} + v_{j,i}\right]. \tag{7}$$

3.2.2. Hydromechanical Numerical Model. Taking into account the efficiency of hydromechanical numerical calculation, the width (x), length (y), and depth (z) of the numerical model were 140, 200, and 70 m, respectively (Figure 5). The top surface of the numerical model was free in all directions. The bottom part of the numerical model was fixed, so there were neither horizontal nor vertical movements. Additionally, no horizontal movement was allowed on x-z planes or y-z planes at the boundaries of the hydromechanical numerical model. In the numerical model, both soils and enclosure structures (diaphragm walls) were modelled by the solid elements, and the struts are modelled by beam elements.

A linear elastic-plastic constitutive model described by using the Mohr-Coulomb strength criterion was used to simulate the behavior of soils. Table 1 lists the calculated parameters of soils from laboratory tests. The materials of the struts and diaphragm walls were modelled as linear elastic, and Poisson's ratio and Young's modulus was set to be 0.2 and 30 GPa, respectively.

Soil-structure interaction was modelled by interfaces on both sides of walls. Interfaces in FLAC3D are one sided, and the constitutive model is also described by a linear Coulomb shear-strength criterion. The necessary input parameters of interfaces on both sides of walls in the modelling are the normal stiffness k_n, shear stiffness k_s, cohesive strength c_s, and frictional strength f_s. The normal stiffness k_n is consistent with the shear stiffness k_s, determined by using the following equation [25]:

$$k_n = k_s = \max\left(\frac{K + (4/3)G}{\Delta z_{\min}}\right), \tag{8}$$

where K and G are bulk and shear modulus, respectively, and $\Delta z_{\min}$ is the smallest width of an adjacent zone to the interfaces in the normal direction. When there is a great difference in the stiffness of the two materials on both sides of the interface, K and G are determined from the softer material, and the interface stiffness is 10 times larger than the softer-side stiffness [25].

3.2.3. Simulation Procedure. Excavation and support of the air shaft are a dynamic process, and the influence of groundwater seepage is taken into account in numerical simulations. The coupled hydromechanical simulations mainly focused on the deformation behavior of the retaining structures and surrounding soil during deep excavation. The simulation procedure was specified as follows: (a) the

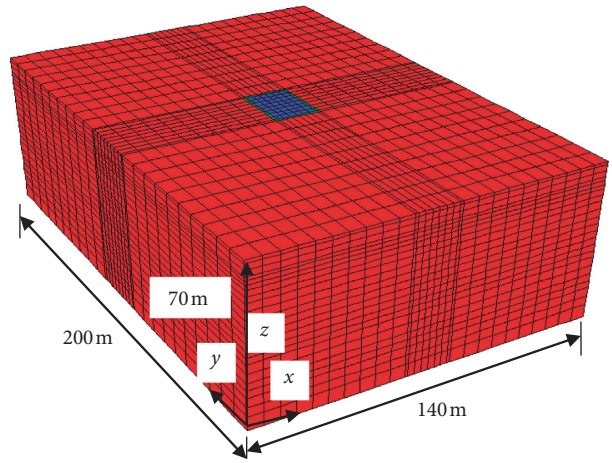

Figure 5: Hydromechanical numerical model.

Table 1: Physicomechanical properties of soils at study site.

Soil layer	Average thickness (m)	Unit weight γ (kN/m^3)	Elastic modulus E (MPa)	Cohesion c (kPa)	Friction angle φ (°)	Hydraulic conductivity k (m/d)
①$_1$ Miscellaneous fill	1.6	18.5	35	5	12	8.5
①$_2$ Plain fill	6.4	18	40	5	10	8.64
②$_5$ Medium-coarse sand	28	19.5	175	2	28	35
③$_1$ Silty clay	1.0	18.6	300	10	20	0.003
③$_8$ Gravel soil	27	21	325	1	35	55
⑦$_1$ Highly weathered granite	—	20.5	600	28	32	0.5

groundwater level inside the enclosure was lowered at 1 m below the bottom of Phase I excavation (Stage 0); (b) excavation and supports were divided into five steps for Phase I excavation of the depth of 23.6 m. The depth of each excavation was 2.5 m, 5.3 m, 5.1 m, 5.2 m, and 5.5 m (Stages S1–S5); (c) underwater excavation without drainage for Phase II excavation was performed in three steps, namely, the excavation depth at each step was 6 m (Stages S6–S8); (d) underwater bottom-sealing concrete of C35 grade was constructed (Stage S9); and (e) C20 concrete was filled into the excavation (Stage S10).

3.2.4. Numerical Prediction of Soil Deformation. Figures 6(a) and 6(b) display the deformation of soil at two major stages of the whole numerical simulation process of the air shaft, respectively. It can be seen that soil deformation is relatively small, with the magnitude of millimeter at the end of dewatering excavation (Phase I excavation). Two possible reasons account for this conclusion: firstly, the total excavation area of the air shaft is only 394.46 m^2. Such a small excavation has little impact on soil outside the excavation. Secondly, a total of five levels of struts that are made of steel-reinforced concrete are installed to support the 23.6 m deep excavation (Phase I excavation). The soil deformation caused by the excavation is restricted effectively due to these steel-reinforced concrete struts of sufficient stiffness.

During the underwater excavation without drainage (Phase II excavation), the soil deformation gradually increases. The maximum soil deformation increases to 36.7 mm at the end of the excavation, which is about 10 times larger than that at the end of Phase I excavation, located at the lower part of diaphragm walls. The major cause is that lateral deformation at the upper part of the enclosure structures is effectively restrained due to the effect of supports installed (diagonal bracing and normal bracing) during the Phase I excavation. Instead, the Phase II excavation of the air shaft is conducted by the means of underwater excavation without drainage. There is no strut at the depth from 23.6 m to 41.6 m for the excavation. The support of the excavation is weakened to some extent. The lower part of the enclosure structures (from 23.6 m to 41.6 m BGS) is only subjected to the water head, leading to larger deformation of the enclosure structures, but the soil deformation is relatively controllable within a reasonable range. From the numerical prediction results, it can be seen that the impact of the whole excavation of the air shaft on the surrounding environment is little. This also implies that the innovative excavation scenario integrating dewatering excavation and underwater excavation can be employed for the deep excavation of the air shaft.

4. Application and Field Monitoring

4.1. Construction Sequence. As presented in Figure 4, the air shaft excavation of 41.6 m depth was divided into two major phases. The first excavation of 23.6 m depth was performed by means of conventional dewatering excavation (Phase I),

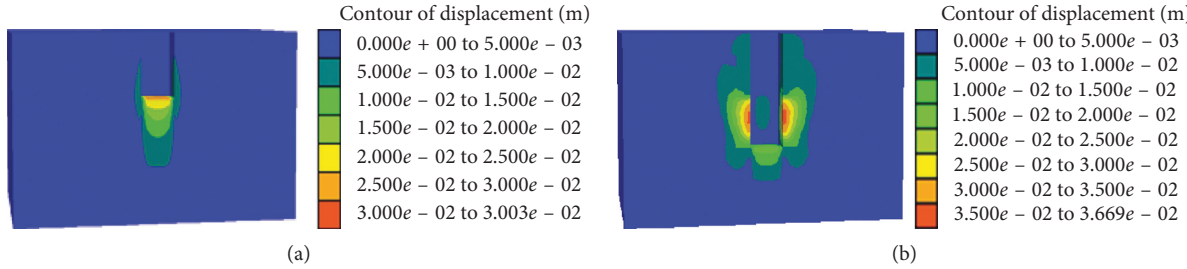

Figure 6: Soil deformation: (a) at the completion of dewatering excavation and (b) at the completion of underwater excavation.

and the second excavation with the depth of 23.6 m to 41.6 m below the ground surface was carried out by underwater excavation without drainage (Phase II). Construction activities were organized into 9 stages (Stage 1 to Stage 9) as shown in Table 2.

Dewatering and braced excavation were used for the excavation of the depth of 23.6 m below the surface (Phase I excavation). Excavation and supports were divided into five steps in total as shown in Figure 4. The dewatering and braced excavation (Phase I excavation) started on August 23, 2016, and completed on November 8, 2016. After the Phase I excavation completed, water was subsequently recharged into the excavation, and the water level inside the enclosure needed to be at least 1 m above the water level outside. Underwater excavation without drainage (Phase II excavation) was conducted until it reached the excavation bottom of the air shaft, completed on December 31, 2016. Then, underwater bottom-sealing concrete and filled concrete are constructed inside the excavation.

4.2. Excavation Implementation

4.2.1. Dewatering Excavation. As presented in Figure 4, braced excavation was used for the excavation of the depth of 23.6 m below the surface (Phase I excavation). Groundwater level inside the enclosure was lowered at 1 m below the bottom of Phase I excavation during the construction. The construction of dewatering and braced excavation was consistent with most of deep excavations [17, 18, 26, 27], which needed no further explanation (shown in Figure 7).

4.2.2. Underwater Excavation without Drainage. Sand-suction machines are used for pumping sand or other sediments inside the excavation when underwater excavation technology is employed for the excavation. Water level inside the excavation remains constant during the underwater excavation. A mixture of silt, sand, and water pumped outside needs to be separated through the sedimentation tank to protect the groundwater environment. Under such condition, pumping water can flow into the backwater area, and water is then pumped into the excavation zone again. By such continuous uninterrupted operations, the underwater excavation without drainage is completed by sand-suction machines. Figure 8(a) displays the actual construction of underwater excavation without drainage at site.

The geotechnical investigation indicated the geology at the upper part in Phase II excavation (about 14 m thick soil) was mainly composed of sandy sediments. At first, the conventional vacuum suction pump was used for pumping sand, but the total volume of sand pumped was only 150–200 m^3 every day. The efficiency of pumping sand was comparatively low. Due to several such advantages as simple operation and high safety factor, a cutter-suction pump was employed for the underwater excavation to improve the efficiency of pumping sand (shown in Figure 8(b)). The pipe of cutter-suction pump was moved inside the enclosure by using a crane during the construction. The daily volume of sand pumped out increased to be about 450 m^3 by the way of cutter-suction pump, which was 3 times as much as before. This improved the work efficiency and saved construction period greatly.

After the work of pumping sandy sediments in the air shaft was completed, the suction of the gravel soil was required. However, there was about 0.5–1 m thick silty clay overlying the gravel soil inside the excavation. Bottlenecks often occurred at the beginning of the excavation due to big viscosity in the water-rich clay. Work on the excavation of the air shaft was quite slow in this situation, and the daily volume of pumped silty clay was only 10 m^3. Worse still, the underlying gravel soil in the air shaft could not be pumped out. To solve this problem, water cannons were replaced with multistage pumps. By this way, silty clay inside the excavation was scoured more efficiently. Besides, cutter-suction pump was changed to vacuum suction pump with a larger diameter. After construction technique and equipment for the underwater excavation without drainage was modified, the work efficiency of pumping clay and gravel was improved remarkably. The daily volume of pumped clay and gravel sediments inside the excavation increased to 90 and 130 m^3, respectively, which indicated that the operation efficiency was greatly improved.

During the construction of underwater excavation without drainage, sediments sometimes covered the surface of diaphragm walls, and even blind spots of the excavation existed inside the air shaft. In these cases, sand-suction machines were unable to pump sediments effectively. Thus, divers were required to dive into the water and to cooperate with the operation of machines at this point. Water cannons were used by them to remove sediments attached to diaphragm walls. Also, the depth of the excavation bottom of the air shaft is needed to be checked by the divers.

Table 2: Construction schedule for the excavation.

Stage	Construction activities	Period (month/day/year)
S1	Excavation to 2.5 m BGS (soil layer 1) and bracing struts at 1.4 m BGS (level 1)	08/23/2016–08/27/2016
S2	Dewatering excavation to 7.8 m BGS (soil layer 2) and bracing struts at 6.5 m BGS (level 2)	08/28/2016–09/10/2016
S3	Dewatering excavation to 12.9 m BGS (soil layer 3) and bracing struts at 11.7 m BGS (level 3)	09/11/2016–09/26/2016
S4	Dewatering excavation to 18.1 m BGS (soil layer 4) and bracing struts at 16.9 m BGS (level 4)	09/27/2016–10/13/2016
S5	Dewatering excavation to 23.6 m BGS (soil layer 5) and bracing struts at 23.6 m BGS (level 5)	10/14/2016–11/08/2016
S6	Underwater excavation without drainage to 41.6 m BGS	11/09/2016–12/31/2016
S7	Underwater bottom-sealing concrete construction	01/01/2017–01/06/2017
S8	Filled concrete construction	01/07/2017–01/10/2017
S9	Casting of the base slabs	01/11/2017–01/24/2017

(a) (b)

Figure 7: Dewatering and braced excavation.

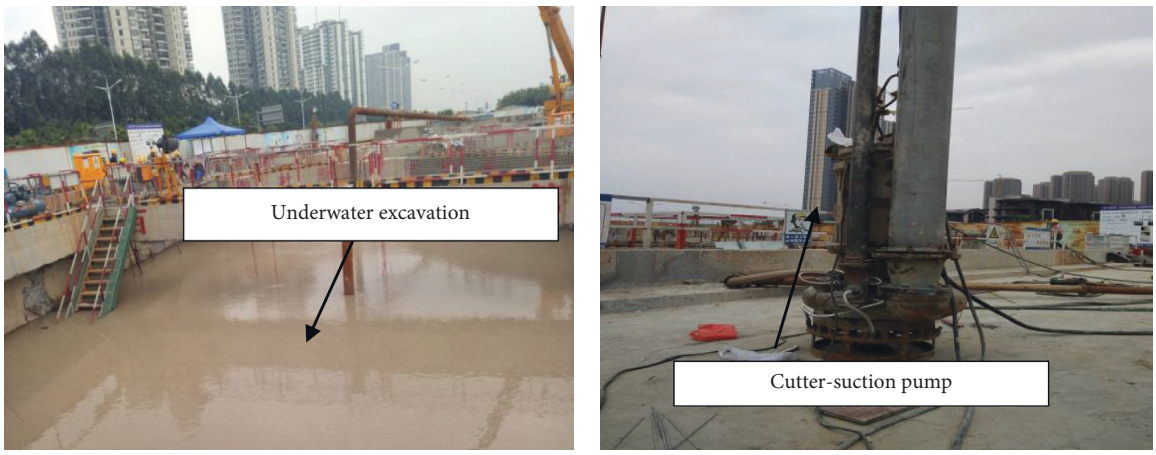

(a) (b)

Figure 8: Construction of underwater excavation. (a) Underwater excavation without drainage. (b) Cutter-suction pump.

4.2.3. Construction of Underwater Bottom-Sealing and Filled Concrete. For TBMs tunneling through the air shaft, the construction of underwater bottom-sealing and filled concrete needed to be carried out after the underwater excavation without drainage completed. The designed thickness of underwater bottom-sealing and filled concrete was 4 m and 15.2 m, respectively. Due to large thickness of filled concrete inside the excavation, construction was divided into two parts, namely, the thickness of each part was 9.8 m and 5.4 m, respectively.

Considering a small excavation area of the air shaft, six pipes made of the seamless steel tube with the inner diameter of 300 mm were employed for the construction of underwater bottom-sealing and filled concrete. Each pipe was composed of several short pipes with the length of 6 m, 3 m, 2 m, and 1 m, respectively. These short pipes were joined with screwed joints and rubber seal rings. The operation platform composed of the I-shaped steel of 45C and 30C, and 3 mm thick steel plate was installed on the struts at Level 2 (shown in Figure 9). The platform allowed the pipes to be moved, and in this case, the time for casting underwater concrete could also be saved. The shaped steel of H20 was installed with each pipe, fixed with the operation platform by welding.

Before underwater bottom-sealing and filled concrete casting, divers were needed to dive to the excavation bottom and to check the depth of the pipe installed when necessary. After the construction of bottom-sealing and backfilling of the air shaft was completed, water was pumped from the air shaft inside to outside. Finally, the base slab of the air shaft (at the bottom of Phase I excavation) was constructed.

4.3. Field Monitoring and Discussion

4.3.1. Instrumentation. Because of the uncertainty and complexities of deep excavations, the existing analytical and numerical methods cannot fully simulate the various uncertain factors and complicated change in actual engineering construction. Generally, in situ monitoring during the construction, immediate evaluation of results, and facilitating rapid response are basic ideas of underground construction. Therefore, no underground construction can be performed without an appropriate monitoring plan. Figure 10 displays the instrumentation locations. The monitoring items during the excavation include (1) groundwater level outside the excavation measured by using water-level gauges (WS1–WS4); (2) ground surface settlement outside the excavation measured by a level instrument (D1–D10); (3) lateral wall displacement measured using inclinometers embedded in the wall; and (4) axial force of 5 concrete struts at each level measured by a stress meter (TZL1-1–TZL1-5 at Level 1, TZL2-1–TZL2-5 at Level 2, TZL3-1–TZL3-5 at Level 3, TZL4-1–TZL4-5 at Level 4, and TZL5-1–TZL5-5 at Level 5). All the instrumentations were attentively calibrated and frequently checked during the monitoring in case of inaccurate measurements when air shaft excavated.

4.3.2. Variation in Groundwater Level. Figure 11 shows the variation of groundwater drawdown outside the air shaft during the whole excavation. It can be seen from Figure 11 that the water level outside the excavation had little fluctuation during the whole construction. The drawdown outside ranged from −0.5 to 0.8 m (positive value indicated a decrease in groundwater level, and negative value suggested water level rise). Pumping in the enclosure had little impact on the drawdown outside during the Phase I excavation. The primary cause was that deep enclosure (55 m deep diaphragm walls) prevented water inflow from outside the excavation. Additionally, clay between sand and gravel sediments had low hydraulic conductivity. These reduced the possibility of groundwater flowing into the excavation and also avoided excessive drawdown outside.

4.3.3. Ground Surface Settlement. Figure 12 displays the ground surface settlement outside the air shaft during the whole excavation. As can be seen from Figure 12, the ground surface basically subsided as the air shaft was excavated, but sometimes a rebound in the soil occurred during the excavation due to water level increase induced by rainfall or tidal effect. The settlement of both the observation points D8 and D9 was larger than that of other observation points around the air shaft throughout the excavation. The maximum settlement of ground surface outside the air shaft was 15 mm when underwater bottom-sealing concrete construction was completed. This indicated that this air shaft constructed by means of combined dewatering excavation and underwater excavation without drainage had little impact on the surroundings.

4.3.4. Lateral Wall Deflection. The observed maximum lateral deflection of diaphragm walls during construction appeared at the monitoring point P9, located at the middle of the west wall. Figure 13 presents the lateral deflections of diaphragm walls at the monitoring point P9 at the completion of two major construction stages (dewatering excavation S5 and underwater excavation without drainage S6). It can be seen that lateral wall deflection has the law of large in the middle part and small at both ends of diaphragm walls during excavation. After dewatering and braced excavation to 23.6 m BGS (Stage S5), the maximum lateral wall deflection δ_{hm} is 19.9 mm. After the completion of underwater excavation without drainage (Stage S6), the maximum lateral wall deflection δ_{hm} increases to about 30 mm, which is still an acceptable value.

4.3.5. Axial Force of Struts. Figures 14(a) and 14(b) display the development of the axial force of struts at Level 2 and Level 4, respectively. The axial force of the rest of the struts develops similarly during the excavation, so they are not shown here to save space. From an overall perspective, the axial force of struts increased as the dewatering and braced excavation (Stage S1–S5) were conducted. The maximum axial force of struts is about 4500 kN, which is an acceptable value. Meanwhile, the axial force of normal bracing struts is

(a) (b)

Figure 9: Construction of underwater bottom-sealing and filled concrete.

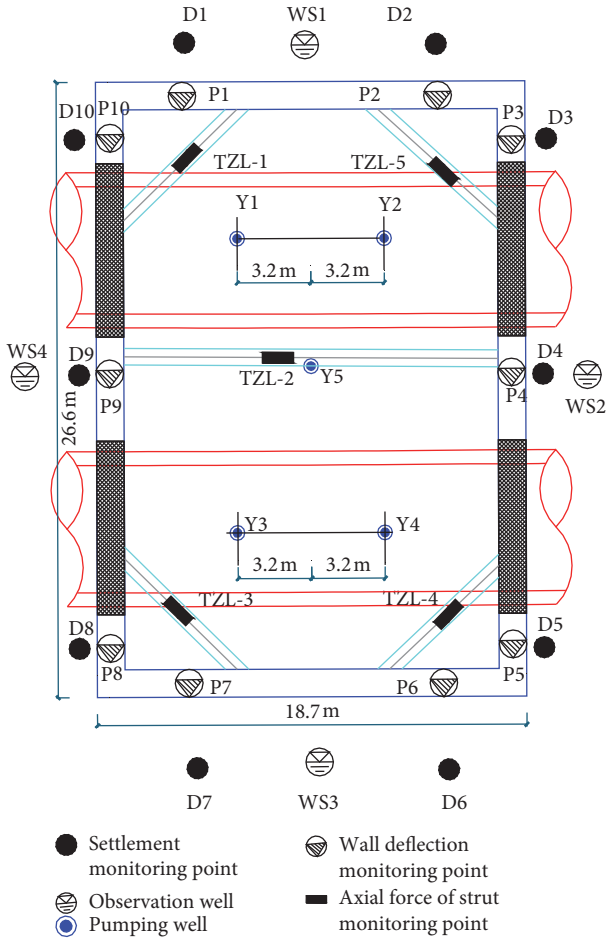

Figure 10: Instrumentation locations.

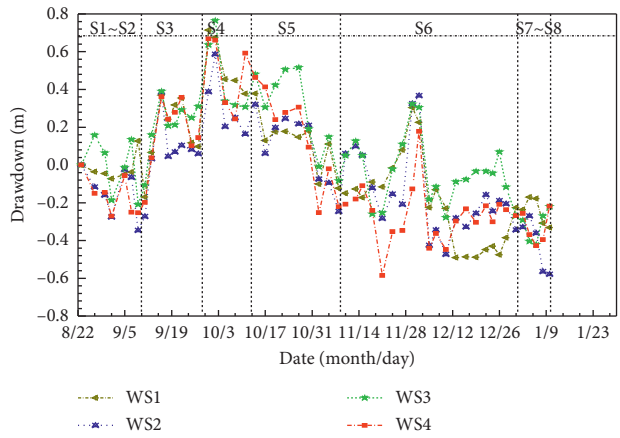

Figure 11: Variation of groundwater drawdown outside the excavation.

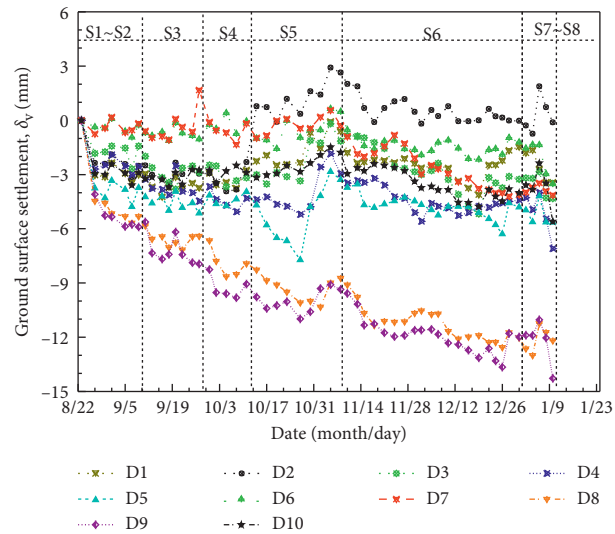

Figure 12: Relationship between ground settlement versus time.

greater than those of diagonal bracing struts at the same level. However, when the underwater excavation without drainage was performed (Stage S6), the axial force of normal bracing struts at both Level 2 and Level 4 was smaller than those during the construction of dewatering and braced

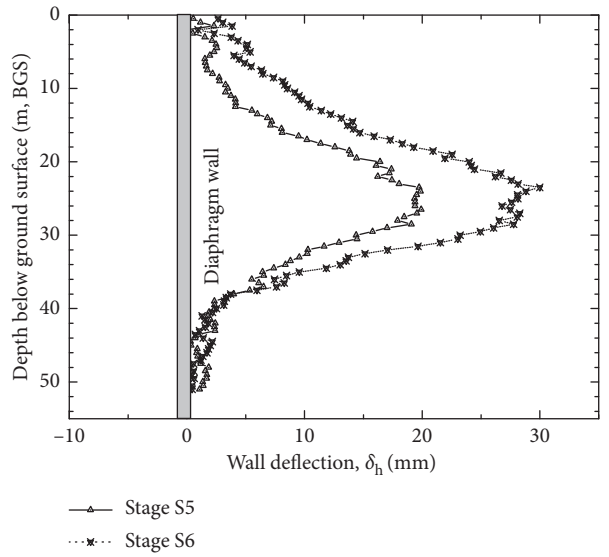

Figure 13: Typical lateral wall deflection.

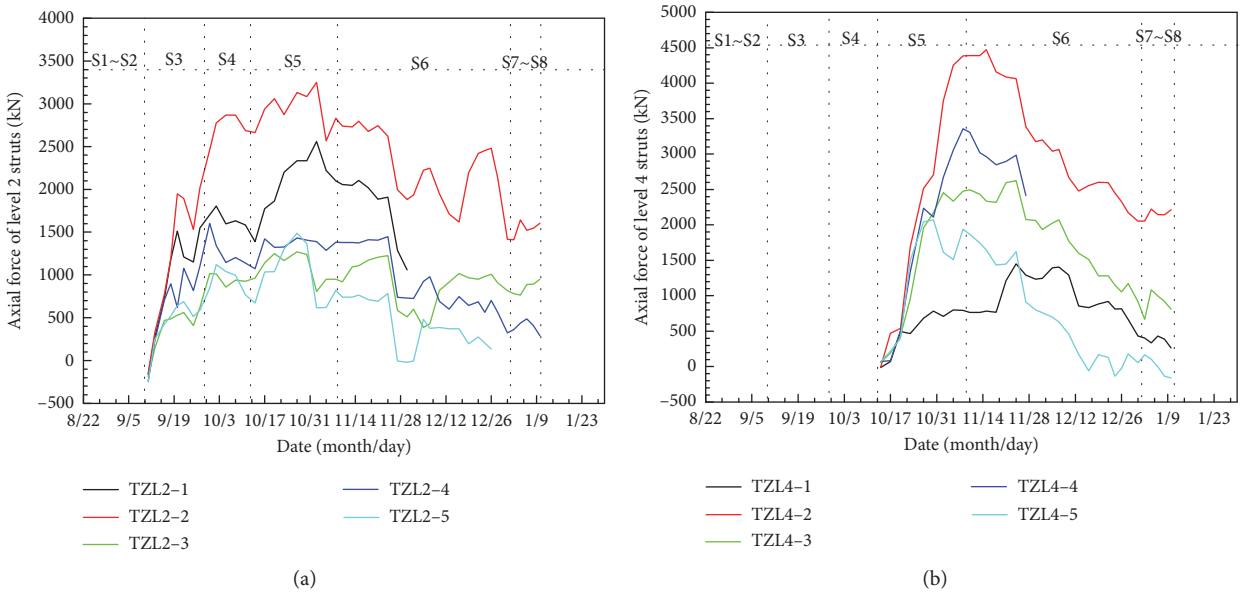

Figure 14: Development of axial force of struts. (a) Level 2. (b) Level 4.

excavation. The main probable cause is that the hydraulic pressure acting on the side wall of diaphragm walls plays a part of the supporting role.

4.3.6. Discussion. Dewatering is usually essential to be performed to ensure dry and workable conditions, as well as to prevent the excavation bottom uplift or liquefaction during the excavation when deep excavations inevitably built below the water table. Currently, dewatering systems composed of diaphragm walls and pumping wells are commonly designed for deep excavations that are undertaken in confined or unconfined aquifers. However, dewatering can sometimes induce environmental problems, especially when diaphragm walls cannot effectively cut off the aquifers. Thus, this innovative scenario that integrates dewatering excavation and underwater excavation without drainage technique presented in this study is maybe an excellent alternative for deep excavations that are undertaken in ultrathick aquifers. The following section mainly discusses the performance of this deep shaft excavation when using this proposed innovative excavation technique.

Figure 15 presents the relationship between the maximum ground surface settlement δ_{vm} and the excavation depth H_e. The δ_{vm}/H_e values in this case ranged from 0.03% to 0.1%, around the lower boundary value ($\delta_{vm} = 0.05\%\ H_e$) reported by Chen et al. [3]. These δ_{vm}/H_e values were much smaller than the boundary ($\delta_{vm} = 0.25\%\ H_e$) of the central cylindrical shaft excavation reported by Tan and Wang [4].

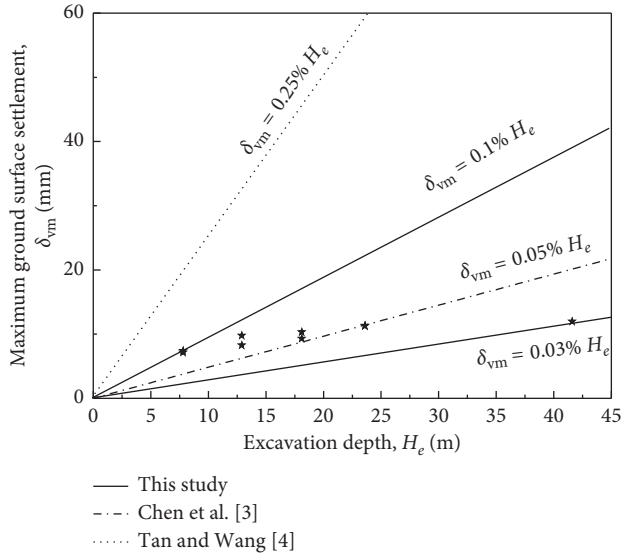

Figure 15: Maximum ground settlement δ_{vm} versus excavation depth H_e.

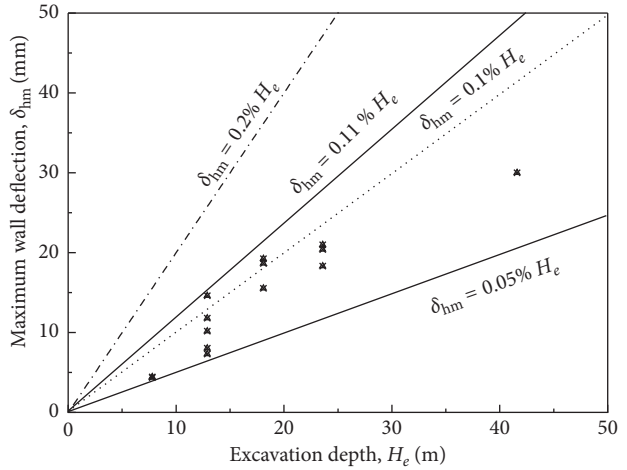

Figure 16: Maximum lateral wall deflection δ_{hm} versus excavation depth H_e.

The main reason is that the excavation of the air shaft is small enough. The impact of such a small excavation on the ground settlement was less than that induced by large-sized excavation.

Figure 16 displays the relationship between the maximum lateral wall deflection δ_{hm} and the excavation depth H_e. The measured wall deflections were relatively small. The measured maximum lateral wall deflection δ_{hm} was around 0.05% H_e to 0.11% H_e. Clough and O'Rourke [28] suggested that δ_{hm}/H_e was around 0.2% with the upper bound of 0.5%. Ou et al. [17] also concluded that δ_{hm}/H_e generally ranged from 0.2% to 0.5% by means of summarizing many historical cases. Tan and Wang [4] proposed the boundaries of δ_{hm} were around 0.1% H_e to 1.0% H_e and 0.02% H_e to 0.5% H_e for the basement excavations and metro excavations in Shanghai soft clay, respectively. All the measured wall deflections fell below the lower boundary proposed by Clough and O'Rourke [28] and Ou et al. [17]. Most of them fell below the lower boundary for the basement excavations in Shanghai soft clay (i.e., 0.1% H_e) reported by Tan and Wang [4]. Thus, measured wall deflections were also less than that predicted by empirical methods, suggesting that wall deflection induced by dewatering excavation and underwater excavation without drainage was limited. That was to say, the diaphragm walls were strong enough and were able to ensure safety of the deep air shaft while constructed by this innovative excavation technique.

The comparisons between field data and results predicted by empirical methods illustrate that this innovative excavation combining dewatering excavation and underwater excavation without drainage is successful while used for excavating the air shaft. On the one hand, it avoided the risk of deep excavation, such as large settlement induced by excessive pumping inside or soil being dragged toward the excavation due to defects in diaphragm walls; on the other hand, the cost and time of excavation was saved. This scenario reduced the schedule of the excavation for the air shaft by more than 2 months. As a consequence, this innovative scenario proposed in this study can also be an alternative for the excavations that undertook deep aquifers when groundwater control is difficult for deep excavations. Additionally, a large-scale excavation can also be separated into several small excavation zones with partition walls when conducted in deep aquifers composed of cohesionless soils. In this way, underwater excavation without drainage can also be carried out for a large-sized excavation.

5. Conclusions

This paper presents an innovative solution for deep shaft excavation that is undertaken in deep aquifers. Through numerical analyses and field measurements, a number of conclusions can be drawn in this study:

(1) Pumping test results imply there is much challenge in lowering the water level inside to ensure dry and workable conditions for the shaft excavation when using conventional dewatering excavation. An innovative excavation technique combining dewatering excavation and underwater excavation without drainage is proposed for the shaft excavation that is undertaken in ultrathick aquifers.

(2) Numerical prediction results show that the soil deformation outside caused by the excavation is little during the dewatering excavation period due to these steel-reinforced concrete struts of sufficient stiffness. Although the soil deformation developed larger than before during underwater excavation, the soil deformation is still relatively controllable within a reasonable range.

(3) Field monitoring results show the maximum settlement of ground surface outside the air shaft is 15 mm when underwater bottom-sealing concrete construction is completed. The ratios of maximum ground surface settlement δ_{vm} to the excavation depth H_e in this case ranged from 0.03% to 0.1%. The maximum lateral wall deflection is 30 mm, and most

of the ratios of maximum lateral wall deflection δ_{hm} to excavation depth H_e are less than 0.1%. All these results are lesser than that predicted by empirical methods, which illustrate that this innovative excavation combining dewatering excavation and underwater excavation without drainage is successful while used for excavating the air shaft.

Data Availability

The data used to support the findings of this study are available from the corresponding author upon request.

Conflicts of Interest

The authors declare that there are no conflicts of interest regarding the publication of this paper.

Acknowledgments

The authors gratefully acknowledge the financial support provided by the National Key R&D Program of China (Grant no. 2017YFB1201204). The authors are grateful for the funds provided by Guangzhou Metro Design & Research Institute Co., Ltd. and CCCC Strait Construction Investment and Development Co., Ltd. The authors also thank the 2nd Harbor Engineering Co., Ltd., of CCCC for cooperation in the field tests and data collection for this study.

References

[1] K. Elbaz, S.-L. Shen, Y. Tan, and W.-C. Cheng, "Investigation into performance of deep excavation in sand covered karst: a case report," *Soils and Foundations*, vol. 58, no. 4, pp. 1042–1058, 2018.

[2] D. Li and C. Yan, "Building deformation prediction based on ground surface settlements of metro-station deep excavation," *Advances in Civil Engineering*, vol. 2018, Article ID 6050353, 14 pages, 2018.

[3] H. Chen, J. Li, and L. Li, "Performance of a zoned excavation by bottom-up technique in Shanghai soft soils," *Journal of Geotechnical and Geoenvironmental Engineering*, vol. 144, no. 11 Article ID 05018003, 2018.

[4] Y. Tan and D. Wang, "Characteristics of a large-scale deep foundation pit excavated by the Central-Island technique in Shanghai soft clay. I: bottom-up construction of the central cylindrical shaft," *Journal of Geotechnical and Geoenvironmental Engineering*, vol. 139, no. 11, pp. 1875–1893, 2013.

[5] Y. Tan and D. Wang, "Characteristics of a large-scale deep foundation pit excavated by the Central-Island technique in Shanghai soft clay. II: top-down construction of the peripheral rectangular pit," *Journal of Geotechnical and Geoenvironmental Engineering*, vol. 139, no. 11, pp. 1894–1910, 2013.

[6] R. A. Forth, "Groundwater and geotechnical aspects of deep excavations in Hong Kong," *Engineering Geology*, vol. 72, no. 3-4, pp. 253–260, 2004.

[7] D. Roy and K. E. Robinson, "Surface settlements at a soft soil site due to bedrock dewatering," *Engineering Geology*, vol. 107, no. 3-4, pp. 109–117, 2009.

[8] C.-H. Shi, C.-Y. Cao, M.-F. Lei, L.-M. Peng, and J. Jiang, "Optimal design and dynamic control of construction dewatering with the consideration of dewatering process," *KSCE Journal of Civil Engineering*, vol. 21, no. 4, pp. 1161–1169, 2017.

[9] Y.-X. Wu, S.-L. Shen, H.-N. Wu, Y.-S. Xu, Z.-Y. Yin, and W.-J. Sun, "Environmental protection using dewatering technology in a deep confined aquifer beneath a shallow aquifer," *Engineering Geology*, vol. 196, pp. 59–70, 2015.

[10] Y.-Q. Zhang, J.-H. Wang, J.-J. Chen, and M.-G. Li, "Numerical study on the responses of groundwater and strata to pumping and recharge in a deep confined aquifer," *Journal of Hydrology*, vol. 548, pp. 342–352, 2017.

[11] Y.-S. Xu, S.-L. Shen, L. Ma, W.-J. Sun, and Z.-Y. Yin, "Evaluation of the blocking effect of retaining walls on groundwater seepage in aquifers with different insertion depths," *Engineering Geology*, vol. 183, pp. 254–264, 2014.

[12] J.-J. Chen, L. Zhang, J.-F. Zhang, Y.-F. Zhu, and J.-H. Wang, "Field tests, modification, and application of deep soil mixing method in soft clay," *Journal of Geotechnical and Geoenvironmental Engineering*, vol. 139, no. 1, pp. 24–34, 2013.

[13] P. Castaldo, F. Jalayer, and B. Palazzo, "Probabilistic assessment of groundwater leakage in diaphragm wall joints for deep excavations," *Tunnelling and Underground Space Technology*, vol. 71, pp. 531–543, 2018.

[14] P. Croce and G. Modoni, "Design of jet-grouting cut-offs," *Proceedings of the Institution of Civil Engineers—Ground Improvement*, vol. 11, no. 1, pp. 11–19, 2007.

[15] C. Cao, C. Shi, and M. Lei, "A simplified approach to design jet-grouted bottom sealing barriers for deep excavations in deep aquifers," *Applied Sciences*, vol. 9, no. 11, p. 2307, 2019.

[16] M. S. Pakbaz, S. Imanzadeh, and K. H. Bagherinia, "Characteristics of diaphragm wall lateral deformations and ground surface settlements: case study in Iran-Ahwaz metro," *Tunnelling and Underground Space Technology*, vol. 35, pp. 109–121, 2013.

[17] C.-Y. Ou, P.-G. Hsieh, and D.-C. Chiou, "Characteristics of ground surface settlement during excavation," *Canadian Geotechnical Journal*, vol. 30, no. 5, pp. 758–767, 1993.

[18] C.-Y. Ou, P.-G. Hsieh, and Y.-L. Lin, "Performance of excavations with cross walls," *Journal of Geotechnical and Geoenvironmental Engineering*, vol. 137, no. 1, pp. 94–104, 2011.

[19] E. Pujades, E. Vázquez-Suñé, J. Carrera et al., "Deep enclosures versus pumping to reduce settlements during shaft excavations," *Engineering Geology*, vol. 169, pp. 100–111, 2014.

[20] E. Pujades, J. Carrera, E. Vázquez-Suñé, A. Jurado, V. Vilarrasa, and E. Mascuñano-Salvador, "Hydraulic characterization of diaphragm walls for cut and cover tunnelling," *Engineering Geology*, vol. 125, pp. 1–10, 2012.

[21] E. Pujades, A. Jurado, J. Carrera, E. Vázquez-Suñé, and A. Dassargues, "Hydrogeological assessment of non-linear underground enclosures," *Engineering Geology*, vol. 207, pp. 91–102, 2016.

[22] J. Wang, B. Feng, T. Guo, L. Wu, R. Lou, and Z. Zhou, "Using partial penetrating wells and curtains to lower the water level of confined aquifer of gravel," *Engineering Geology*, vol. 161, no. 3, pp. 16–25, 2013.

[23] J. Wang, X. Liu, Y. Wu et al., "Field experiment and numerical simulation of coupling non-Darcy flow caused by curtain and pumping well in foundation pit dewatering," *Journal of Hydrology*, vol. 549, pp. 277–293, 2017.

[24] Y.-X. Wu, S.-L. Shen, and D.-J. Yuan, "Characteristics of dewatering induced drawdown curve under blocking effect of

retaining wall in aquifer," *Journal of Hydrology*, vol. 539, pp. 554–566, 2016.

[25] Itasca, *FLAC3D v. 3.1–Fast Lagrangian Analysis of Continua in Three dimensions. User Manual*, Itasca Consulting Group, Minneapolis, MN, USA, 2006.

[26] R. J. Finno, S. Bryson, and M. Calvello, "Performance of a stiff support system in soft clay," *Journal of Geotechnical and Geoenvironmental Engineering*, vol. 128, no. 8, pp. 660–671, 2002.

[27] R. J. Finno and M. Calvello, "Supported excavations: observational method and inverse modeling," *Journal of Geotechnical and Geoenvironmental Engineering*, vol. 131, no. 7, pp. 826–836, 2005.

[28] G. W. Clough and T. D. O'Rourke, "Construction induced movements of in-situ walls," in *Design and Performance of Earth Retaining Structures*, pp. 439–470, ASCE, Reston, VA, USA, 1990.